Exact Nonlinear Dynamic Analysis of a Beam With a Nonlinear Vibration Absorber and With Various Boundary Conditions

Mohammad Bukhari
Department of Mechanical Engineering
Virginia Tech,
Blacksburg, VA 24061

Oumar Barry[1]
Department of Mechanical Engineering
Virginia Tech,
Blacksburg, VA 24061
e-mail: obarry@vt.edu

We study the nonlinear vibration of a beam with an attached grounded and ungrounded nonlinear vibration absorber (NVA) using the exact natural frequencies and mode shapes of the loaded beam. The nonlinearity in the beam is due to midplane stretching and that in the NVA is of cubic stiffness nonlinearity. We consider various boundary conditions and derive their closed-form characteristic equations and mode shapes. The method of multiple scales (MMS) is directly applied to the nonlinear partial differential equations of motion to obtain explicit expressions of the nonlinear frequency, modulation, and loci of the saddle-node bifurcation equations. Our analytical approach is validated using direct numerical simulation. Parametric studies demonstrate that the performance of the NVA does not only depend on its key design variables and location, but also on the boundary conditions, midplane stretching of the beam, and type of configuration (i.e., grounded NVA versus ungrounded NVA). Our analysis also indicates that the use of common approach such as employing approximate modes in estimating the nonlinear response of a loaded beam produces significant error (i.e., up to 1200% in some case). These observations suggest that the exact modes shape and natural frequencies are required for a precise investigation of the nonlinear dynamic of loaded beams. These findings could contribute to the design improvement of NVAs, microelectromechanical systems (MEMS), energy harvesters, and metastructures. [DOI: 10.1115/1.4045287]

Keywords: midplane stretching, nonlinear vibration absorber (NVA), perturbation methods, nonlinear frequency, stability, ungrounded and grounded NVAs, exact mode shapes, loaded beam, various boundary conditions

1 Introduction

Vibration absorbers (VAs), consisting of mass–spring–damper system, have been studied for many years. VAs can be linear or nonlinear. When properly tuned, linear VAs can provide a simple and cost-effective way for passive vibration control. However, mistuning drastically deteriorates their performance [1] and multiple linear VA devices may be required given their narrowband operation.

The narrowband restriction of linear VAs can be overcome by means of nonlinear vibration absorbers (NVAs) also known as nonlinear energy sinks when they lack a linear element [1,2]. NVAs are robust to variations in structural properties and have broadband vibration mitigation capacity [2]. NVAs can be very effective in controlling many types of unwanted vibrations including wind-induced vibration of power lines [3], and flutter instability of suspension bridges [4] and airplane wings [5–7].

Airplane wings, overhead power lines, suspension cable bridges, microelectromechanical systems (MEMS), and many other engineering applications can be modeled as beams. When the beam exhibits large amplitude deformation, linear theory can no longer hold. One must resort to nonlinear theory to characterize the nonlinear vibration of the beam.

One of the earlier considerations of nonlinear vibrations of beam was introduced by Woinowsky-Krieger [8]. Similar problems were considered by Burgreen to study the free vibration of a hinged column [9]. Burgreen supported his analytical results through experiment. Bennett [10] considered the effect of viscous damping on the ultraharmonic motion of a hinged beam. The stability and response were both studied using the harmonic balance method.

The nonlinear oscillation of beams was reviewed by Nayfeh and Mook [11]. Nayfeh also reviewed perturbation techniques used to solve weakly nonlinear problems [12]. The nonlinear vibrations of a beam with a grounded NVA without damping were introduced for the first time by Dowell [13]. He examined the free vibrations of this nonlinear problem with simply supported boundary conditions. Pakdemirli and Nayfeh [14] extended Dowell's work by investigating the forced vibration problem (i.e., external primary resonance case) and including the nonlinearity in the beam due to midplane stretching and by adding damping in the grounded NVA. This work was also extended by Barry et al. [15] by considering the effect of axial load and multigrounded spring–mass–damper systems, and Bukhari and Barry [16] by including the effect of the mass rotational inertia effect.

[1]Corresponding author.

Contributed by the Design Engineering Division of ASME for publication in the Journal of Computational and Nonlinear Dynamics. Manuscript received April 15, 2019; final manuscript received October 14, 2019; published online November 11, 2019. Assoc. Editor: Mohammad Younis.

Numerous authors have examined the nonlinear vibration of beams carrying multimasses with different boundary conditions [17–21], nonlinear beam with nonideal boundary conditions [22], and cracked cantilever beam on elastic supports [23]. Moreover, the nonlinear vibrations of microbeam in different MEMS systems have been studied extensively in Refs. [24–27]. Furthermore, the nonlinear vibration of structure with bolted joints can be found in Ref. [28].

The nonlinear vibration of a beam with an ungrounded spring–mass system was also investigated in Refs. [29–31]; however, the nonlinearity was only due to spring stiffness. Moreover, the study of autoparametric NVA attached to linear discrete system can be found in Refs. [32–34]. Avramov and Gendelman [35] have employed the nonlinear normal modes to solve the nonlinear problem due the midplane stretching. However, they used the mode shapes of the bare beam to tackle the problem rather than those of the loaded beam (i.e., combined beam and spring–mass system). Other nonlinear vibration studies focusing on rotating beam with spring-mass system can be found in Refs. [36–38]. However, the effect of suspended mass, external force, and end constraints was not considered.

Many studies have been reported in the literature focusing on nonlinear vibration of a beam with in-span grounded NVAs (i.e., the spring is fixed to the ground at one end and connected to the attached in-span mass at the other end; hence, there is no coupling between the beam and mass). However, they all used the approximate modes of the bare beam to predict the nonlinear dynamic of the loaded beam. Also, to the best of our knowledge, there are no works that examined how boundary conditions and midplane stretching nonlinearity affect the performance of an ungrounded or grounded NVA. This problem is examined for the first time in this paper using the exact natural frequencies and mode shapes of the loaded beam. The study of ungrounded nonlinear absorbers is motivated by Stockbridge dampers, which are passive vibration control devices used to suppress wind-induced vibration of power lines or suspension bridge cables [3,39]. The stiffness nonlinearity of a Stockbridge damper is generally of a cubic type [39].

Inspired by Stockbridge dampers, this study assumes that the stiffness of the NVA is of cubic nonlinearity. It is also assumed that the nonlinearity in the beam is due to midplane stretching because of the movement restriction at its ends. The beam is also subjected to external primary resonance excitation. The main contribution of this work is as follows: (1) application of the multiple scales method directly to the nonlinear governing equations of motion to obtain analytical solutions; (2) presentation of explicit expressions for the characteristic equation and mode shapes of the loaded beam under various boundary conditions and the use of these exact modes in our analysis; and (3) performance comparison of ungrounded NVA versus grounded NVA with and without damping. It should be noted that the method of multiple scales (MMS), albeit a little more involved, has advantages over other methods as it can better handle coupled systems and damped systems [40]. The obtained analytical results are validated via comparison with those in the literature and via direct numerical simulation. Parametric studies are carried out to examine the influence of key design variables, midplane stretching nonlinearity, and boundary conditions on the performance of grounded and ungrounded NVAs.

2 Mathematical Model

Figure 1 illustrates schematic diagrams of the system with different cases of boundary conditions. The system consists of an Euler–Bernoulli beam with a spring–mass–damper system attached to the beam at $x_1 = x_{s1}$. The beam has a length L, a mass per unit length m, a flexural rigidity EI, and an axial rigidity EA. The spring–mass system has a total mass M, a linear stiffness k, and a cubic nonlinear stiffness q. Two reference frames are defined at the ends of the beam to simplify the algebra, thus obtaining explicit expressions of the mode shapes and frequency equations of the loaded beam.

The Lagrangian for the total system can be obtained as

$$\mathcal{L} = \sum_{i=1}^{2}\int_0^{x_{si}} m\dot{W}_i^2 dx_i + M\dot{v}^2 - \frac{1}{2}\sum_{i=1}^{2}\int_0^{x_{si}} \mathrm{EI}\left(W_i''\right)^2 dx_i - \frac{1}{2}\sum_{i=1}^{2}\int_0^{x_{si}} \mathrm{EA}\left(u_i' + \frac{1}{2}W_i'^2\right)^2 - \frac{1}{2}K(W_1(x_{s1},t) - v)^2 - \frac{1}{4}q(W_1(x_{s1},t) - v)^4 \tag{1}$$

where u_i and w_i are the transverse and axial beam displacement, respectively, $x_{s2} = L - x_{s1}$. The dots and primes denote differentiation with respect to time and space, respectively.

Introducing the Lagrangian into Hamilton's principle and adding the dashpot damping leads to the following two equations of motion and four continuity conditions:

$$m\ddot{W}_i + \mathrm{EI}W_i^{iv} = \frac{\mathrm{EA}}{2L}\left[\sum_{r=1}^{2}\int_0^{x_{sr}} W_r'^2 dx_r\right]W_i'' \tag{2}$$

$$M\ddot{V} = K(W_1(x_{s1},t) - V) + q(W_1(x_{s1},t) - V)^3 + C_d(\dot{W}_1(x_{s1},t) - \dot{V}) \tag{3}$$

$$W_1(x_{s1},t) = W_2(x_{s2},t) \tag{4}$$

$$W_1'(x_{s1},t) = -W_2'(x_{s2},t) \tag{5}$$

$$W_1''(x_{s1},t) = W_2''(x_{s2},t) \tag{6}$$

$$\mathrm{EI}[W_1'''(x_{s1},t) + W_2'''(x_{s2},t)] = K(W_1(x_{s1},t) - V) + q(W_1(x_{s1},t) - V)^3 + C_d(\dot{W}_1(x_{s1},t) - \dot{V}) \tag{7}$$

The boundary conditions for each case are listed in Appendix. For convenience, we introduce the following dimensionless variables:

$$\xi_i = \frac{x}{L};\quad \xi_{si} = \frac{x_{si}}{L};\quad w_i = \frac{W_i}{L};\quad \tau = \frac{t}{l^2}\sqrt{\frac{\mathrm{EI}}{m}};\quad \alpha = \frac{M}{mL};\quad k = \frac{KL^3}{\mathrm{EI}};\quad \gamma = \frac{qL^5}{\mathrm{EI}};\quad \lambda = \frac{AL^3}{I};\quad v = \frac{V}{L};\quad \bar{c}_d = C_d L\sqrt{\frac{1}{m\mathrm{EI}}} \tag{8}$$

Using the dimensionless parameters, Eqs. (2)–(7) become

$$\ddot{w}_i + w_i^{iv} = \frac{1}{2}\lambda\left[\sum_{r=1}^{2}\int_0^{\xi_{sr}} w_r'^2 d\zeta_r\right]w_i'' \tag{9}$$

$$\alpha\ddot{v} = k(w_1(\xi_{s1},\tau) - v) + \gamma(w_1(\xi_{s1},\tau) - v)^3 + \bar{c}_d(\dot{w}_1(\xi_{s1},\tau) - \dot{v}) \tag{10}$$

$$w_1(\xi_{s1},\tau) = w_2(\xi_{s2},\tau) \tag{11}$$

$$w_1'(\xi_{s1},\tau) = -w_2'(\xi_{s2},\tau) \tag{12}$$

$$w_1''(\xi_{s1},\tau) = w_2''(\xi_{s2},\tau) \tag{13}$$

$$w_1'''(\xi_{s1},\tau) + w_2'''(\xi_{s2},\tau) = k(w_1(\xi_{s1},\tau) - v) + \gamma(w_1(\xi_{s1},\tau) - v)^3 + \bar{c}_d(\dot{w}_1(\xi_{s1},\tau) - \dot{v}) \tag{14}$$

where the dots and primes denote differentiation with respect to time and displacement, respectively. By adding forcing and internal damping terms, Eq. (9) becomes

$$\ddot{w}_i + w_i^{iv} = \frac{1}{2}\lambda\left[\sum_{r=1}^{2}\int_0^{\xi_{sr}} w_r'^2 d\zeta_r\right] w_i'' - 2\bar{\mu}\dot{w}_i + \bar{F}_i \cos\Omega t \quad (15)$$

where $\bar{\mu}$, $\bar{F}$, and ω are the dimensionless damping coefficient, the dimensionless force amplitude, and the dimensionless excitation frequency, respectively.

By using the method of multiple scales, the expansions of the displacements for Eqs. (10)–(15) are assumed as

$$w_i(\xi_i, \tau, \epsilon) = \epsilon w_{i1}(\xi_i, T_0, T_2) + \epsilon^3 w_{i3}(\xi_i, T_0, T_2) + \cdots \quad (16)$$

$$v(\tau, \epsilon) = \epsilon v(T_0, T_2) + \epsilon^3 v(T_0, T_2) + \cdots \quad (17)$$

where ϵ is a bookkeeping parameter and it has a small dimensionless value, $T_0 = \tau$ represents a fast-time scale, and $T_2 = \epsilon^2\tau$ is a slow-time scale. Since the nonlinearity appears at order ϵ^3 the scale T_1 does not exist in the expansions. In this study, we aim at tackling the primary resonance case, so we let $\bar{\mu} = \epsilon^2\mu$, $\bar{c}_d = \epsilon^2 c_d$, and $\bar{F} = \epsilon^2 F_i$, such that the effect of damping, nonlinearity, and excitation appears in the same perturbation equations.

The dimensionless time derivatives in terms of partial derivatives with respect to T_n can be expressed as

$$(\cdot) = D_0 + \epsilon^2 D_2 \quad (18)$$

$$(\cdot\cdot) = D_0^2 + 2\epsilon^2 D_0 D_2 \quad (19)$$

where $D_n = \partial/\partial T_n$.

Substituting Eqs. (16)–(19) into Eqs. (10)–(15), and collecting the coefficient of similar power on both sides lead to*order* ϵ

$$D_0^2 w_{i1} + w_{i1}^{iv} = 0 \quad (20)$$

$$w_{11}(\xi_{s1}, \tau) = w_{21}(\xi_{s2}, \tau) \quad (21)$$

$$w_{11}'(\xi_{s1}, \tau) = -w_{21}'(\xi_{s2}, \tau) \quad (22)$$

$$w_{11}''(\xi_{s1}, \tau) = w_{21}''(\xi_{s2}, \tau) \quad (23)$$

$$w_{11}'''(\xi_{s1}, \tau) + w_{21}'''(\xi_{s2}, \tau) = k(w_{11}(\xi_{s1}, \tau) - v_1) \quad (24)$$

$$\alpha\ddot{v}_1 = k(w_{11}(\xi_{s1}, \tau) - v_1) \quad (25)$$

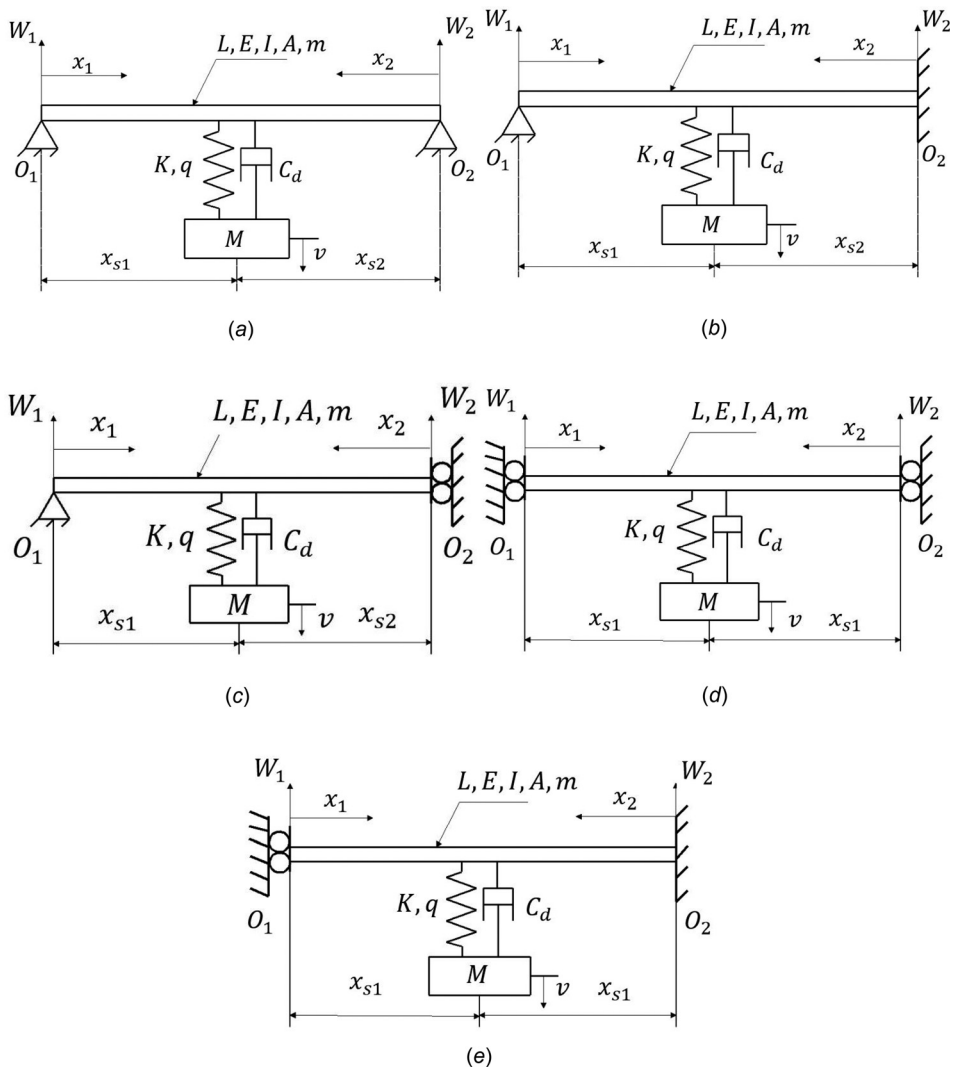

Fig. 1 Schematic diagram for the beam with NVA for different boundary conditions: (*a*) pinned-pinned, (*b*) pinned-clamped, (*c*) pinned-guided, (*d*) guided-guided, and (*e*) guided-clamped

order ϵ^3

$$D_0^2 w_{i3} + w_{i3}^{iv} = \frac{1}{2}\lambda\left[\sum_{r=1}^{2}\int_0^{\xi_{sr}} w_{r1}'^2 d\zeta_r\right] w_{i1}'' - 2\epsilon^2 D_0 D_2 w_{i1} - 2\mu D_0 w_{11} + F_i \cos\Omega T_0 \tag{26}$$

$$w_{13}(\xi_{s1},\tau) = w_{23}(\xi_{s2},\tau) \tag{27}$$

$$w_{13}'(\xi_{s1},\tau) = -w_{23}'(\xi_{s2},\tau) \tag{28}$$

$$w_{13}''(\xi_{s1},\tau) = w_{23}''(\xi_{s2},\tau) \tag{29}$$

$$w_{13}'''(\xi_{s1},\tau) + w_{23}'''(\xi_{s2},\tau) = k(w_{13}(\xi_{s1},\tau) - v_3) + \gamma(w_{11}(\xi_{s1},\tau) - v_1)^3 + c_d(\dot{w}_{13}(\xi_{s1},\tau) - \dot{v}_3) \tag{30}$$

$$\alpha\ddot{v}_3 = k(w_{13}(\xi_{s1},\tau) - v_3) + \gamma(w_{11}(\xi_{s1},\tau) - v_1)^3 + c_d(\dot{w}_{13}(\xi_{s1},\tau) - \dot{v}_3) \tag{31}$$

3 Linear Problem

For Eqs. (20)–(25) at order ϵ, the problem is linear. Since the linear system models are free harmonic vibrations, the solution of the displacements can be assumed following [41] as:

$$w_{i1} = [A_1(T_2)e^{j\omega T_0} + \text{cc}]Y_i(\xi_i) \tag{32}$$

$$v_1 = A_2(T_2)e^{j\omega T_0} + \text{cc} \tag{33}$$

where cc represents the complex conjugate for the preceding terms. Substituting Eqs. (32) and (33) into Eqs. (20)–(25) yields

$$Y_i^{iv} - \omega^2 Y_i = 0 \tag{34}$$

$$Y_1(\xi_{s1}) = Y_2(\xi_{s2}) \tag{35}$$

$$Y_1'(\xi_{s1}) = -Y_2'(\xi_{s2}) \tag{36}$$

$$Y_1''(\xi_1) = Y_2''(\xi_2) \tag{37}$$

$$Y_1'''(\xi_{s1}) + Y_2'''(\xi_{s2}) = k\left(Y_1(\xi_{s1}) - \frac{A_2}{A_1}\right) \tag{38}$$

$$-\alpha\omega^2 A_2 = k(A_1 Y_1(\xi_{s1}) - A_2) \tag{39}$$

We should note here that the boundary conditions are presented in Appendix. From Eq. (39), one can obtain

$$A_2 = \Psi Y_1(\xi_{s1})A_1 \tag{40}$$

where Ψ is defined as

$$\Psi = \frac{k}{k - \alpha\omega^2} \tag{41}$$

The mode shapes of each beam segment can be defined as

$$Y_1(\xi_1) = c_{11}\sin\beta\xi_1 + c_{21}\cos\beta\xi_1 + c_{31}\sinh\beta\xi_1 + c_{41}\cosh\beta\xi_1 \tag{42}$$

$$Y_2(\xi_2) = c_{12}\sin\beta\xi_2 + c_{22}\cos\beta\xi_2 + c_{32}\sinh\beta\xi_2 + c_{42}\cosh\beta\xi_2 \tag{43}$$

where c_{ij} is an arbitrary constant that is defined in Appendix for all studied boundary conditions. The natural frequencies of the linear system can be determined from Eq. (38) after substituting the values of c_{ij} from Appendix.

4 Nonlinear Problem

At order ϵ^3, the equations are nonlinear. The homogeneous solutions of Eqs. (26)–(31) are free from secular terms; however, the inhomogeneous solutions of the right-hand side are not. To have a solution for the latter case, the secular terms must be eliminated by satisfying the solvability condition. First, we need to obtain this condition by expressing the solutions in the form of

$$w_{i3} = \phi_i(\xi_i, T_2)e^{j\omega T_0} + \text{cc} + W_i^*(\xi_i, T_0, T_2) \tag{44}$$

$$v_3 = A_3(T_2)e^{j\omega T_0} + \text{cc} + V^* \tag{45}$$

where W_i^* and V^* are unique, free of secular terms, and small divisor terms. In case of primary resonance, the excitation frequency is close to one of the natural frequencies of the total system, so the excitation frequency can be expressed as

$$\Omega = \omega + \epsilon^2\sigma \tag{46}$$

where σ is a detuning parameter. Substituting Eqs. (32) and (33), Eqs. (40) and (41), and Eqs. (44)–(46) into Eqs. (26)–(31), and collecting the coefficient of e^{jwT_0} in order to eliminate the secular terms yields

$$\phi_i^{iv} - \omega^2\phi_i = \frac{3}{2}\lambda\bar{A}_1 A_1^2\left[\sum_{r=1}^{2}\int_0^{\xi_{sr}} Y_r'^2(\xi_r)d\zeta_r\right] Y_i''(\xi_s i) - 2j\omega(A_1' + \mu A_1)Y_i(\xi_{si}) + \frac{1}{2}F_i e^{j\sigma T_2} \tag{47}$$

$$\phi_1(\xi_{s1},T_2) = \phi_2(\xi_{s2},T_2) \tag{48}$$

$$\phi_1'(\xi_{s1},T_2) = -\phi_2'(\xi_{s2},T_2) \tag{49}$$

$$\phi_1''(\xi_{s1},T_2) = \phi_2''(\xi_{s2},T_2) \tag{50}$$

$$\phi_1'''(\xi_{s1},T_2) + \phi_2'''(\xi_{s2},T_2) = k(\phi_1(\xi_{s1},T_2) - A_3) + 3\gamma\Psi_1 A_1^2\bar{A}_1 Y_1^3(\xi_{s1}) + j\omega c_d(A_1 Y_1(\xi_{s1}) - A_2) \tag{51}$$

$$-\alpha\omega^2 A_3 + 2j\omega\alpha A_2' = k(\phi_1(\xi_{s1},T_2) - A_3) + 3\gamma\Psi_1 A_1^2\bar{A}_1 Y_1^3(\xi_{s1}) + j\omega c_d(A_1 Y_1(\xi_{s1}) - A_2) \tag{52}$$

where Ψ_1 is defined as

$$\Psi_1 = -3\Psi^3 + 9\Psi^2 - 9\Psi + 1 \tag{53}$$

Rearranging Eq. (52) results in

$$A_3 = \frac{3\gamma\Psi_1 A_1^2\bar{A}_1 Y_1^3(\xi_{s1}) + k\phi_1(\xi_{s1},T_2) - 2j\omega\alpha\Psi A_1' Y_1(\xi_{s1})}{k - \alpha\omega^2} + \frac{j\omega c_d A_1 Y_1(\xi_{s1})(1-\Psi)}{k - \alpha\omega^2} \tag{54}$$

Using Eqs. (41) and (54), Eq. (51) can be expressed as

$$\phi_1'''(\xi_{s1},T_2) + \phi_2'''(\xi_{s2},T_2) = k(\phi_1(\xi_{s1},T_2)(1-\Psi) - 3\Psi_2 A_1^2\bar{A}_1 + j\omega\Psi_3 A_1' - j\omega\Psi_4 A_1(1-\Psi)) + 3\gamma\Psi_1 A_1^2\bar{A}_1 Y_1^3(\xi_{s1}) + j\omega c_d Y_1(\xi_{s1})A_1(1-\Psi) \tag{55}$$

where Ψ_2 and Ψ_3 are given by

$$\Psi_2 = \frac{\gamma \Psi_1 Y_1(\xi_{s1})^3}{k - \alpha\omega^2} \tag{56}$$

$$\Psi_3 = \frac{2\alpha \Psi Y_1(\xi_1)}{k - \alpha\omega^2} \tag{57}$$

$$\Psi_4 = \frac{c_d Y_1(\xi_{s1})}{k - \alpha\omega^2} \tag{58}$$

Manipulating Eqs. (47)–(51) yields

$$\begin{aligned} &2j\omega\left(A_1' + \mu A\right)b_1 + 3\bar{A}_1 A_1^2\left(-\frac{\lambda}{2}b_2 b_3 - kY_1(\xi_{s1})\Psi_2 + \gamma\Psi_1 Y_1^4(\Psi_{s1})\right) \\ &+ j\omega k Y_1(\xi_{s1})\Psi_3 A_1' - j\omega Y_1(\xi_{s1})k\psi_4 A_1(1-\Psi) \\ &+ j\omega c_d Y_1(\xi_{s1})A_1(1-\Psi) - \frac{1}{2}fe^{j\sigma T_2} = 0 \end{aligned} \tag{59}$$

where the constants b_1, b_2, b_3, and f are

$$b_1 = \sum_{r=1}^{2}\int_0^{\xi_{sr}} Y_r^2 d\xi_r \tag{60}$$

$$b_2 = \sum_{r=1}^{2}\int_0^{\xi_{sr}} Y_r'^2 d\xi_r \tag{61}$$

$$b_3 = \sum_{r=1}^{2}\int_0^{\xi_{sr}} Y_r'' Y_r d\xi_r \tag{62}$$

$$f = \sum_{r=1}^{2}\int_0^{\xi_{sr}} F_r Y_r d\xi_r \tag{63}$$

Integrating b_3 by parts and applying the boundary conditions yields $b_3 = -b_2$.

It is more convenient to introduce A_1 in the polar form as

$$A_1(T_2) = \frac{1}{2}a(T_2)e^{j\theta(T_2)} \tag{64}$$

In order to transfer Eq. (59) into an autonomous form, the following expression should be assumed:

$$\gamma_1 = \sigma T_2 - \theta \tag{65}$$

Substituting Eqs. (64) and (65) into Eq. (59), and separating the real and imaginary parts yield

$$\omega a' b_4 = \frac{1}{2}f\sin\gamma_1 - \omega b_6 a \tag{66}$$

$$\omega a\left(\sigma - \gamma_1'\right)b_4 = -\frac{1}{2}f\cos\gamma_1 + a^3 b_5 \tag{67}$$

where b_4 and b_5 are defined as

$$b_4 = b_1 + \frac{1}{2}Y_1(\xi_{s1})\Psi_3 k \tag{68}$$

$$b_5 = \frac{3}{16}\lambda b_2^2 - \frac{3}{8}k\Psi_2 Y_1(\xi_{s1}) + \frac{3}{8}\gamma\Psi_1 Y_1^4(\xi_{s1}) \tag{69}$$

$$b_6 = \mu b_1 + Y_1(\xi_{s1})\left[-\frac{1}{2}k\Psi_4(1-\Psi) + \frac{1}{2}c_d Y_1(\xi_{s1})(1-\psi)\right] \tag{70}$$

In order to calculate nonlinear frequencies, we assume free undamped vibrations. This can be obtained by letting $\sigma = f = \mu = 0$, then

$$a' = 0 \Rightarrow a = \text{constant} \tag{71}$$

$$\omega a b_4 \gamma_1' = -b_5 a^3 \tag{72}$$

Therefore, the nonlinear frequency is obtained as

$$\omega_{\text{nl}} = \omega\theta' \frac{b_5 a^2}{\omega b_4} \tag{73}$$

where

$$\theta' = \frac{b_5 a^2}{\omega b_4} = \theta_r a^2 \tag{74}$$

and θ_r is defined as the correction factor.

Since a is a constant, the motion is periodic. Therefore, $a' = \gamma_1' = 0$. By eliminating γ_1 from Eqs. (66) and (67), the detuning parameter can be obtained as

$$\sigma = \frac{a^2 b_5}{\omega b_4} \pm \sqrt{\frac{f^{*2}}{4a^2\omega^2} - \mu^{*2}} \tag{75}$$

where

$$f^* = \frac{f}{b_4};\ \mu^* = \frac{b_6}{b_4} \tag{76}$$

The locus of the vertical tangents to the frequency response curve can be found by solving the following equation:

$$\sigma^2 - 4\frac{a^2 b_5}{\omega b_4}\sigma + 3\frac{a^4 b_5^2}{\omega^2 b_4^2} + \mu^{*2} = 0 \tag{77}$$

Finally, it is noteworthy that we only analyze the cubic nonlinearity case because as many other investigators have confirmed, beam midplane stretching nonlinearities [14] and weakly nonlinear vibration absorbers [5,42,43] can be approximated using cubic order nonlinearity. The addition of higher order nonlinear terms (e.g., quantic) can be analyzed in a similar way using the method of multiple scales but considering higher order perturbation, or other asymptotic techniques such as the method of normal forms or homotopy perturbation method [44].

5 Numerical Simulation

5.1 Nonlinear Frequencies. The natural frequencies of the linear system can be obtained by solving Eq. (38). The lowest five

Table 1 The lowest five natural frequencies for pinned-pinned case and for two different values of suspended mass

α	ξ_{s1}	First mode	Second mode	Third mode	Fourth mode	Fifth mode
0.5	0.1	9.2873	19.382	41.506	90.298	159.075
2	0.1	7.089	12.799	41.184	90.298	159.075
0.5	0.2	8.223	20.363	44.656	91.059	158.319
2	0.2	5.464	15.583	43.924	90.964	158.319
0.5	0.3	7.3577	22.777	45.394	89.066	158.319
2	0.3	4.612	18.598	44.522	89.066	158.319
0.5	0.4	6.904	25.934	42.153	89.634	159.075
2	0.4	4.192	21.599	41.635	89.634	159.075
0.5	0.5	6.747	28.011	39.47	91.155	157.942
2	0.5	4.07	23.208	39.47	91.06	157.942

Table 2 The lowest five natural frequencies for pinned-guided case and for two different values of suspended mass

α	ξ_{s1}	First mode	Second mode	Third mode	Fourth mode	Fifth mode
0.5	0.1	2.441	16.545	25.629	63.401	122.158
2	0.1	2.349	9.136	24.084	63.242	122.158
0.5	0.2	2.349	14.497	29.566	65.246	122.047
2	0.2	2.081	8.895	27.484	65.004	122.047
0.5	0.3	2.243	14.119	32.862	63.641	120.945
2	0.3	1.802	9.564	30.333	63.481	120.945
0.5	0.4	2.124	14.996	33.4373	61.662	122.379
2	0.4	1.581	11.006	30.664	61.662	122.379
0.5	0.5	2.009	16.995	30.333	63.561	121.716
2	0.5	1.41	13.304	27.747	63.401	121.716
0.5	0.6	1.911	20.273	26.189	65.246	121.055
2	0.6	1.283	16.626	23.79	65.004	121.055
0.5	0.7	1.843	21.692	25.934	63.481	122.6
2	0.7	1.205	18.857	22.872	63.322	122.49
0.5	0.8	1.789	19.075	31.444	61.662	121.496
2	0.8	1.14	16.667	28.117	61.662	121.496
0.5	0.9	1.749	17.202	34.604	63.8	121.275
2	0.9	1.108	14.88	31.725	63.641	121.275

Table 4 The lowest five natural frequencies for pinned-clamped case and for two different values of suspended mass

α	ξ_{s1}	First mode	Second mode	Third mode	Fourth mode	Fifth mode
0.5	0.1	13.414	21.368	51.804	105.627	179.359
2	0.1	8.137	17.661	51.588	105.627	179.359
0.5	0.2	11.273	24.428	54.28	105.833	178.556
2	0.2	6.566	21.091	53.839	105.833	178.556
0.5	0.3	10.097	27.852	53.619	104.295	178.958
2	0.3	5.796	24.527	53.181	104.295	178.958
0.5	0.4	9.719	30.443	50.446	105.524	178.958
2	0.4	5.534	26.755	50.3745	105.524	178.958
0.5	0.5	9.907	29.621	50.801	105.936	178.423
2	0.5	5.653	25.985	50.73	105.936	178.423
0.5	0.6	10.645	26.138	54.133	104.295	179.359
2	0.6	6.163	22.825	53.692	104.295	179.359
0.5	0.7	11.989	22.777	54.797	105.524	178.289
2	0.7	7.062	19.514	54.354	105.524	178.289
0.5	0.8	13.857	20.363	52.381	106.348	179.359
2	0.8	8.367	16.954	52.165	106.245	179.359
0.5	0.9	15.23	19.603	50.304	104.704	178.824
2	0.9	9.595	15.583	50.233	104.704	178.824

natural frequencies are tabulated in Tables 1–5 for different values of α and ξ_{s1}. In contrast with the results of first mode obtained for a grounded NVA in Refs. [14] and [15], the fundamental natural frequency of the beam with ungrounded NVA decreases as the system moves toward the middle of the beam for all boundary conditions except the guided-guided case. In the guided-guided case, the change in natural frequencies is similar to that of a grounded NVA attached to a beam, which was studied in Refs. [14] and [15]. As expected, increasing the suspended mass reduces the natural frequencies; however, the significance of this reduction is also dependent on the location of the mass–spring system along the beam.

The linear natural frequencies obtained analytically are compared to those in the literature. The results are listed in Table 6 and show very good agreement. The natural frequencies for a bare beam with various boundary conditions are tabulated in Table 7. Comparing the results in Tables 1–5 to those of Table 7 suggest that common approach such as using approximate modes to analyzes the vibration of a loaded beam will lead to erroneous results. Hence to accurately predict the dynamic of a beam with attached NVAs, we should employ the exact modes of the loaded beam rather than those of the bare beam.

The change in nonlinear frequency can be obtained by calculating the correction factor θ_r (i.e., higher correction factor means more nonlinearity). The effect of changing both the location and the mass on the correction factor is depicted in Figs. 2–6. The figures indicate that the nonlinearity increases with moving the suspended system toward the middle of the beam for the case where the vertical displacement of both ends is restricted. However, for other cases (i.e., guided boundary condition), the nonlinearity increases when the suspended system is near the moving boundary condition. The effect of midplane stretching increases the nonlinearity in general, but it reduces the nonlinearity in the guided-guided case. Furthermore, it is demonstrated that increasing the suspended mass reduces the nonlinearity in general. However, a very large suspended mass can increase the nonlinearity at specific locations as shown in Figs. 5 and 6.

The nonlinear frequency curves for different boundary conditions are plotted in Fig. 7 and the results show that replacing the pinned support by guided support reduces the nonlinearity while replacing both supports increase it.

Table 3 The lowest five natural frequencies for guided-guided case and for two different values of suspended mass

α	ξ_{s1}	First mode	Second mode	Third mode	Fourth mode	Fifth mode
0.5	0.1	7.604	27.222	44.924	89.728	158.068
2	0.1	6.313	23.693	43.924	89.634	158.068
0.5	0.2	8.08	28.489	40.418	89.066	158.697
2	0.2	6.878	23.741	40.164	89.066	158.697
0.5	0.3	8.776	25.8827	40.227	90.964	158.697
2	0.3	7.826	20.634	40.037	90.869	158.697
0.5	0.4	9.502	22.161	43.725	90.393	158.068
2	0.4	9.045	16.749	43.001	90.393	158.068
0.5	0.5	9.875	20.68	45.664	88.784	159.201
2	0.5	9.871	14.9402	44.79	88.784	159.201

5.2 Nonlinear Frequency Response Curves. The next numerical analysis focuses on the forced vibration response of the beam-NVA system. The analysis also investigates how key design variables, boundary conditions, and midplane stretching

Table 5 The lowest five natural frequencies for guided-clamped case and for two different values of suspended mass

α	ξ_{s1}	First mode	Second mode	Third mode	Fourth mode	Fifth mode
0.5	0.1	3.715	22.634	38.844	75.995	139.063
2	0.1	2.243	19.691	36.936	75.908	139.063
0.5	0.2	3.851	25.175	33.96	74.693	139.535
2	0.2	2.379	21.321	32.519	74.693	139.535
0.5	0.3	4.07	25.883	30.443	76.694	140.008
2	0.3	2.6	20.408	30.333	76.606	140.008
0.5	0.4	4.379	21.368	34.31	77.22	138.827
2	0.4	2.916	16.626	33.206	77.132	138.827
0.5	0.5	4.72	18.169	38.223	75.039	140.008
2	0.5	3.358	13.377	36.633	75.039	140.008
0.5	0.6	5.074	16.545	38.906	75.299	139.535
2	0.6	3.95	11.106	37.363	75.299	139.535
0.5	0.7	5.371	16.382	36.21	77.66	139.063
2	0.7	4.655	9.781	35.017	77.572	139.063
0.5	0.8	5.534	17.577	32.69	76.957	140.482
2	0.8	5.302	9.379	32.064	76.869	140.363
0.5	0.9	5.581	19.25	30.553	75.039	139.299
2	0.9	5.581	9.688	30.443	75.039	139.299

Table 6 The lowest five natural frequencies of the system for $\xi_{s1} = .25$, $\alpha = .2$, $k = 3$, $M = 15.3875\,\text{kg}$, $L = 1\,\text{m}$, and $EI = 6.34761 \times 10^4\,\text{N.m}^2$

BCs	Data	First mode	Second mode	Third mode	Fourth mode	Fifth mode
Pinned pinned	Present	243.8525	645.2102	2540.6986	5705.9775	10,144.2278
	FEM [45]	243.8579	645.2030	2540.5306	5706.1886	10,142.4012
Pinned clamped	Present	247.1475	993.2784	3212.6601	6698.6082	11,451.0585
	FEM [45]	245.9788	1000.1317	3212.8284	6696.1421	11,449.8613

Table 7 Natural frequencies for different boundary conditions

Case	First mode	Second mode	Third mode	Fourth mode	Fifth mode
Pinned-pinned	9.870	39.478	88.826	157.914	246.740
Pinned-guided	2.467	22.207	61.685	120.903	199.860
Guided-guided	5.272	15.940	33.952	78.000	142.229
Pinned-clamped	15.418	49.965	104.248	178.271	272.032
Guided-clamped	14.397	26.553	65.042	124.318	203.364

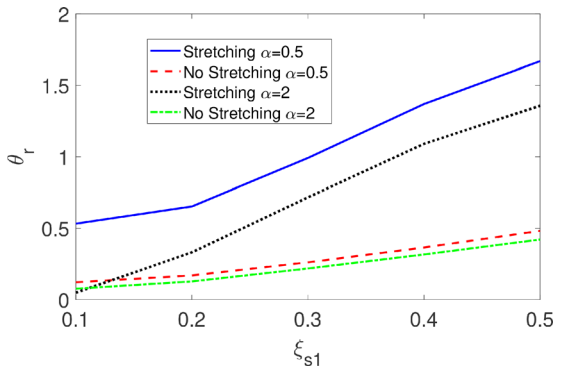

Fig. 2 System location versus correction factor: $k = \gamma = 2\pi^4$, first mode of vibration, pinned-pinned case

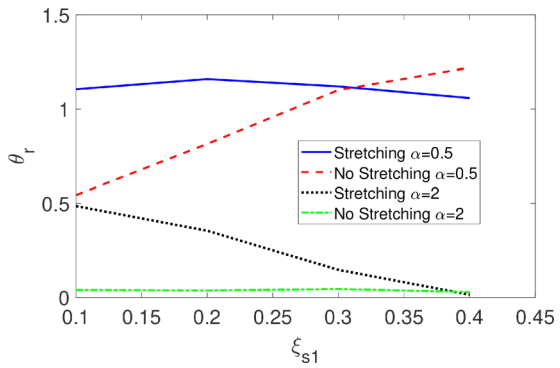

Fig. 4 System location versus correction factor: $k = \gamma = 2\pi^4$, first mode of vibration, guided-guided case

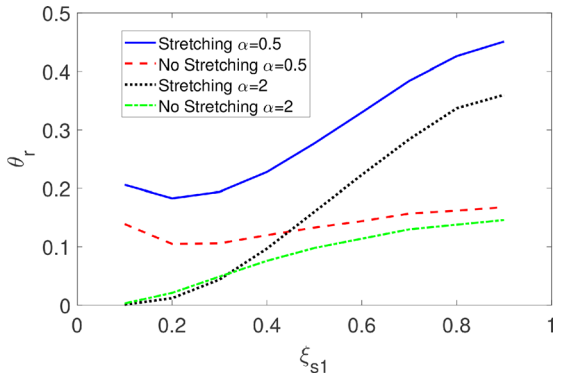

Fig. 3 System location versus correction factor: $k = \gamma = 2\pi^4$, first mode of vibration, pinned-guided case

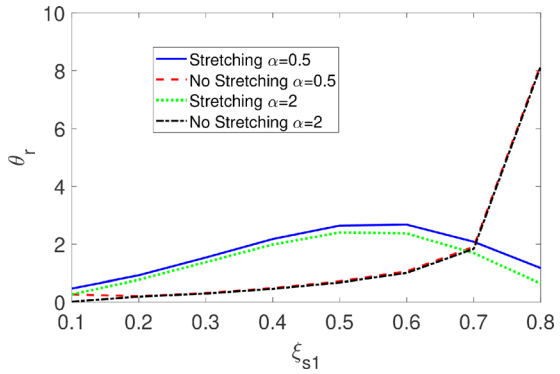

Fig. 5 System location versus correction factor: $k = \gamma = 2\pi^4$, first mode of vibration, pinned-clamped case

nonlinearity affect the performance of grounded and ungrounded NVAs. First, we validate our analytical solution via direct numerical simulation. The results are shown in Fig. 8 and show very good agreement, thus demonstrating that our analytical approach is very accurate.

One of the main contributions of this study is employing the exact vibration modes of the loaded beam and applying MMS directly to the governing equations of motion to obtain the solution of the nonlinear vibration problem. Our present approach can then be compared to the conventional approach of using approximate modes of a bare beam to predict the nonlinear dynamic of a loaded beam. The results of this comparison are depicted in Figs. 9 and 10 and show significant discrepancy between the two approaches. In Fig. 9, the ungrounded NVA is not tuned, whereas it is tuned in Fig. 10. Comparing Figs. 9 and 10 clearly show that the difference between our approach and the common approach is more pronounced when the NVA is tuned. In this case, we observe up to 80% difference in vibration amplitude and up 1200% difference in detuning frequency (Fig. 10). These observations clearly suggest that the exact natural frequencies and

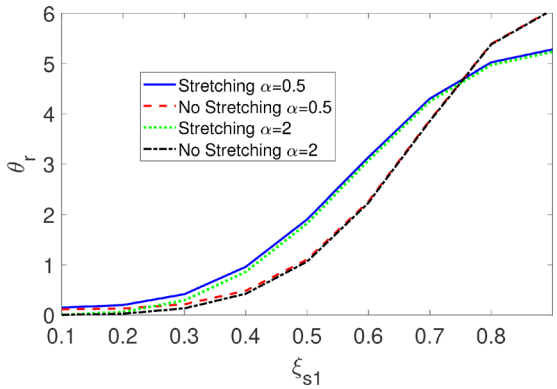

Fig. 6 System location versus correction factor: $k = \gamma = 2\pi^4$, first mode of vibration, guided-clamped case

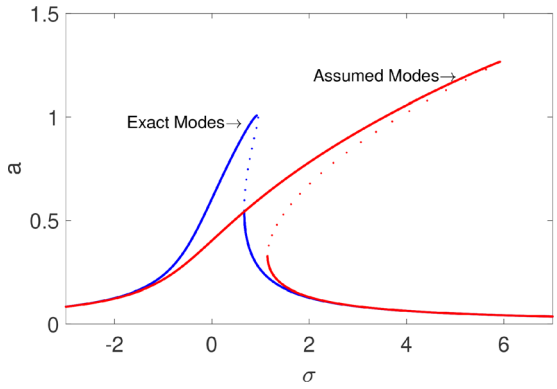

Fig. 9 Comparison between the exact mode and assumed mode solutions when the ungrounded NVA is not tuned $\alpha = 0.25$, $k = 0.0125\pi^4$, $f = 2$, second mode of vibrations, pinned-pinned case

modes shapes of the loaded beam, rather than the approximate modes of the bare beam, should be employed to accurately predict the nonlinear dynamic response of a beam-NVA system.

Figure 11 compares the performance of a grounded and ungrounded NVA with and without damping. In the absence of damping, the results indicate that the vibration amplitude for beam with ungrounded NVA is higher and the multivariable region is narrower. This is an indication that an ungrounded NVA can perform worst in terms of vibration reduction than a grounded configuration. In all frequency response curves, the solid lines represent the stable solutions while the dotted lines refer to unstable solution. In the presence of damping, the results contradict those with the absence of damping, suggesting that with damping, ungrounded NVAs exhibit superior performance than their grounded counterparts. The influence of boundary conditions on the performance of the NVA is depicted in Fig. 12. We can observe that the pinned-guided case has higher displacement and narrow multivariable regions, whereas the guided-guided case exhibits lower vibration amplitudes and wider multivariable regions. Figure 13 shows the corresponding frequency response of

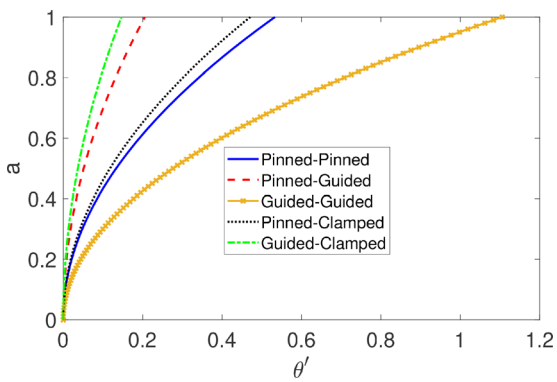

Fig. 7 Nonlinear frequency versus vibration amplitude (with stretching): $k = \gamma = 2\pi^4$, $\alpha = 0.25$, first mode of vibration

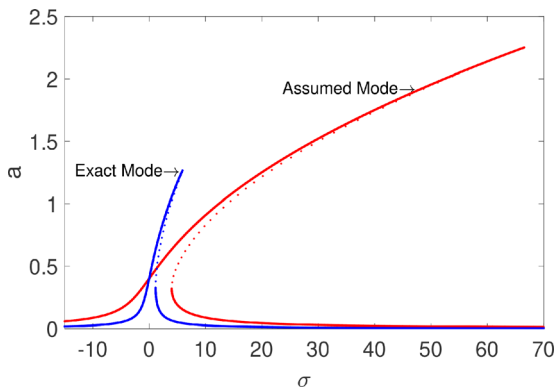

Fig. 10 Comparison between the exact mode and assumed mode solutions when the ungrounded NVA is tuned to the second mode of vibration $\alpha = 0.25$, $k = 0.125\pi^4$, $f = 2$, second mode of vibrations, pinned-pinned case

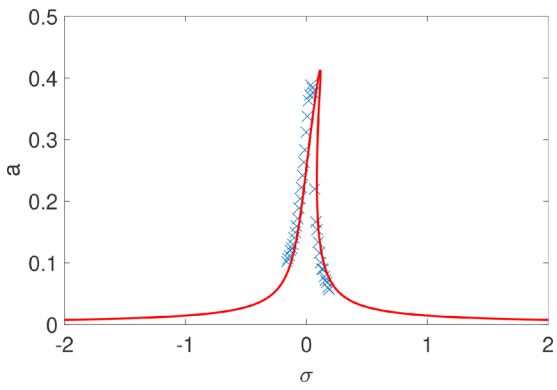

Fig. 8 Validating the exact solution by numerical integration $k = .125\pi^4$, $\gamma = 0.05k$, alpha = 0.25, $f = 0.5$, pinned-pinned case. (-): the method of multible scale; (x): numerical integration.

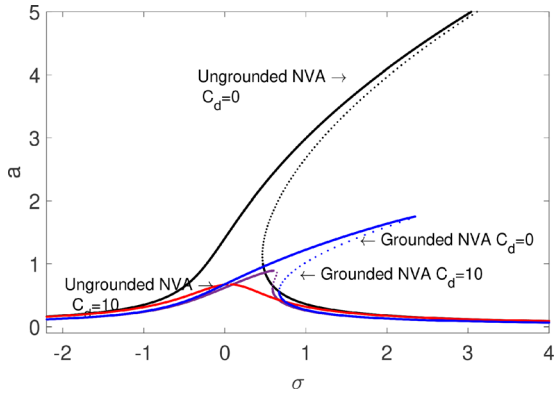

Fig. 11 Detuning parameter versus vibration amplitude (with stretching): $k = \gamma = 2\pi^4$, $\alpha = 2$, $f = 1$, $\xi_{s1} = 1$, $\mu = 0.2$ first mode of vibration, pinned-pinned case

the NVA and confirms the results in Fig. 12. In that, the NVA exhibits best performance (i.e., largest amplitude and widest bandwidth) for the guided-guided case and worst performance (i.e., smallest amplitude and narrowest bandwidth) for the pinned-guided case. Such findings can be explored to improve the design of vibration absorbers, MEMS resonators, energy harvesters, and wave control in metamaterials.

Figures 14–19 depict the effect of the suspended mass on the NVA's performance for various boundary conditions. In the absence of dashpot damping, increasing the mass increases the vibration amplitude for the pinned-pinned boundary conditions as shown in Fig. 14, thus degrading the performance of the NVA. In Fig. 15, we can observe that increasing the mass in the presence of damping can improve or degrade the performance of the NVA for the case of pinned-pinned boundary condition. For all reminder boundary conditions (Figs. 16–19 except for the guided-guided (Fig. 17) and the pinned-guided (Fig. 16) cases, the results show that increasing the suspended mass in the presence of damping can also improve or degrade the performance of the NVA. In the guided-guided case, increasing the suspended mass always improves the performance of NVA, whereas in the pinned-guided case, it degrades the performance of the NVA. The implication

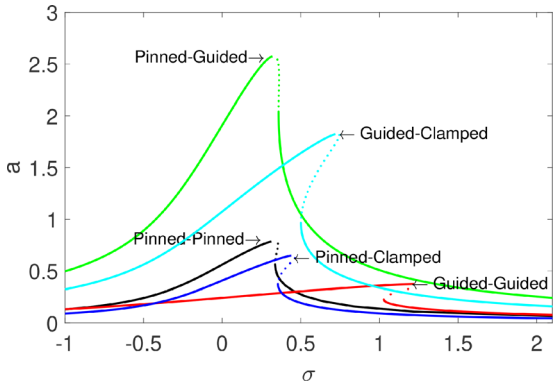

Fig. 12 Frequency–response curves for different end conditions; $\alpha = 0.5$, $f = 2.5$, $k = 2\pi^4$, $c_d = 0$, and $\xi_{s1} = 0.2$ first mode of vibration

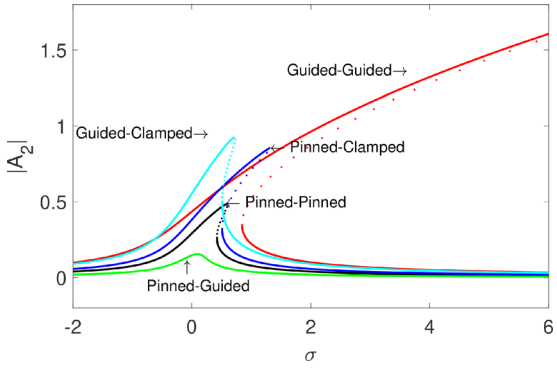

Fig. 13 NVA amplitude for different end conditions; $\alpha = 0.5$, $f = 2.5$, $k = 2\pi^4$, $c_d = 0$, and $\xi_{s1} = 0.2$ first mode of vibration

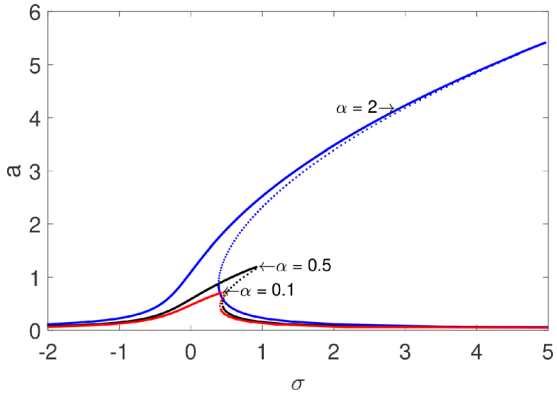

Fig. 14 The effect of increasing the suspended mass on the vibration amplitude (without dashpot damping); $f = 2.5$, $k = 2\pi^4$, $c_d = 0$, and $\xi_{s1} = 0.2$ first mode of vibration, pinned-pinned case

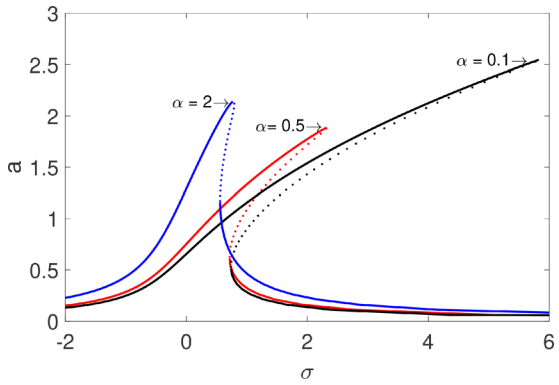

Fig. 15 The effect of increasing the suspended mass on the vibration amplitude (with dashpot damping); $f = 5$, $k = 2\pi^4$, $c_d = 2.5$, and $\xi_{s1} = 0.2$ first mode of vibration, pinned-pinned case

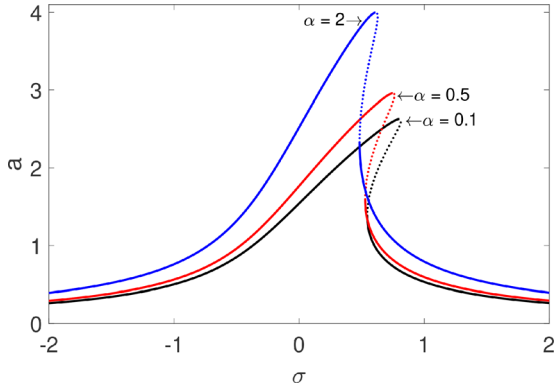

Fig. 16 The effect of increasing the suspended mass on the vibration amplitude (with dashpot damping); $f = 2.5$, $k = 2\pi^4$, $c_d = 5$, and $\xi_{s1} = 0.4$ first mode of vibration, pinned-guided case

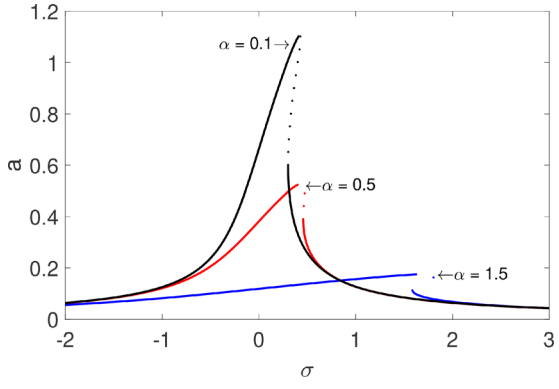

Fig. 17 The effect of increasing the suspended mass on the vibration amplitude (wit dash pot damping); $f = 2.5$, $k = 2\pi^4$, $c_d = 2.5$, and $\xi_{s1} = 0.5$ first mode of vibration, guided-guided case

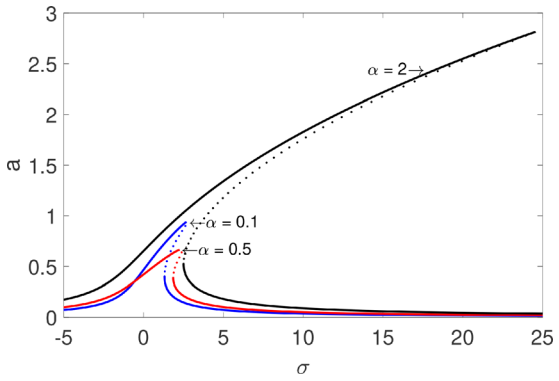

Fig. 18 The effect of increasing the suspended mass on the vibration amplitude (wit dash pot damping); $f = 10$, $k = 2\pi^4$, $c_d = 2.5$, and $\xi_{s1} = 0.5$ first mode of vibration, clamped-pinned case

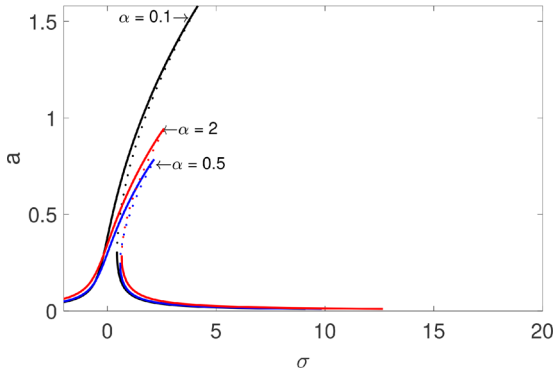

Fig. 19 The effect of increasing the suspended mass on the vibration amplitude (wit dash pot damping); $f = 1$, $k = 2\pi^4$, $c_d = 2.5$, and $\xi_{s1} = 0.6$ first mode of vibration, guided-clamped case

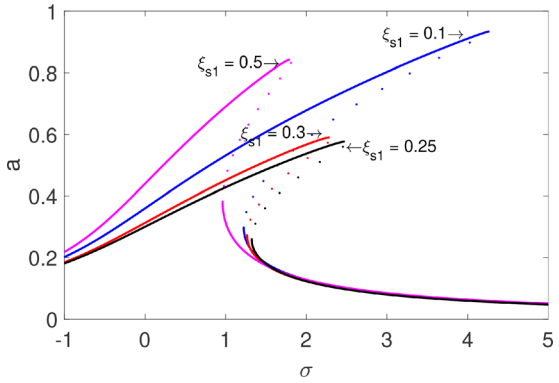

Fig. 20 Optimum location of vibration absorber (with dash pot damping); $f = 2$, $k = \pi^4$, $c_d = 0.2$, and $\alpha = 0.25$ second mode of vibration, pinned-pinned case

here is that the interplay between boundary conditions, absorber mass, and damping should be carefully examined to improve the design of NVAs.

In Fig. 20, we examine how the performance of the NVA is affected by its location along the beam. The results suggest that best performance is achieved when the NVA is located at, or closer to a vibration antinode. It should be noted that the effect of nonlinearity is more dominant at the vibration antinode than the

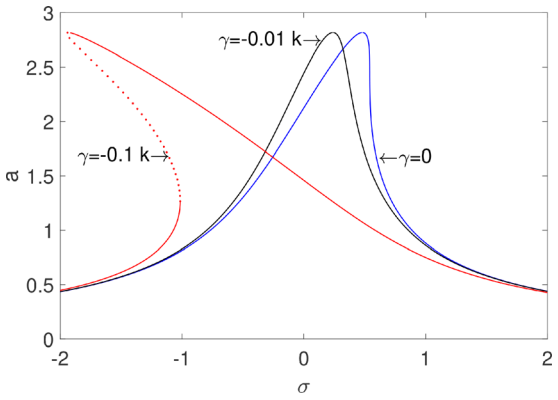

Fig. 21 Effect of softening nonlinearity on frequency response functions; $f = 10$, $k = 2\pi^4$, $c_d = 2.5$, and $\alpha = 2$ first mode of vibration, clamped-pinned case

node. For this specific case (i.e., second mode excitation), placing the NVA at $\xi_{s1} = 0.1$ (closer to node) yields worst performance, whereas placing it at $\xi_{s1} = 0.25$ (antinode) yields best performance.

In Fig. 21, we examine the effect of softening nonlinearity on the frequency response of the beam. The softening nonlinearity was assigned to the NVA. The results of Fig. 21 show that the backbone curve shifts from right to left with increasing softening nonlinearity, thus suggesting that the nonlinearity in the NVA governs the dynamic of the coupled system.

6 Conclusion

This paper analytically studied the nonlinear vibration of a beam with a suspended spring–damper–mass system for different cases of boundary conditions and using the exact natural frequencies and mode shapes of the loaded beam. We considered nonlinearities from midplane stretching of the beam and cubic stiffness of the NVA. Our study was focused on the primary resonance case. The nonlinear problem is tackled by the method of multiple scales. Explicit expressions are presented for the characteristic equation, mode shape, nonlinear frequency, detuning parameter, and loci of the saddle-node bifurcation. The validation of the present results is demonstrated via comparison of the results in the literature and via direct numerical simulation. The numerical simulation indicated that the role of NVA placement ξ_{s1} on the fundamental natural frequency depends on the type of NVA configuration (i.e., grounded versus ungrounded). This finding was consistent in all studied boundary conditions except the guided-guided case. Numerical examples demonstrated that the use of approximate modes can yield up to 1200% error in predicting the nonlinear dynamic of the loaded beam, particularly, when the NVA is tuned. This observation suggests that the exact mode shapes and natural frequencies of the loaded beam should be employed to accurately predict the nonlinear response of a beam with attached NVAs. Parametric studies showed that positioning the NVA at a vibration antinode not only improves the performance of the NVA but also increases the effect of nonlinearity by stretching the hardening frequency response curve more to the right. Moreover, the nonlinearity increases with midplane stretching except for the guided-guided case. In general, this nonlinearity reduces with increasing mass. In the presence of damping, our analysis showed that ungrounded NVAs perform better than their ungrounded counterparts; but the reverse was observed in the absence of damping. In the absence of damping, the maximum vibration amplitude increases, in general, with increasing suspended mass. However, adding damping and increasing the suspended mass resulted in different trends in some of the studied boundary conditions. The performance of the NVA can degrade or improve with varying suspended mass for the pinned-pinned, pinned-clamped, and clamped-guided cases. For the pinned-

guided case, the performance of the absorber improves with decreasing suspended mass; whereas, it degrades for the guided-guided case. These results suggest that the interplay between boundary conditions and absorber's mass, damping, and location is crucial for improving the performance of NVAs. The findings in this paper can also be very useful for improving the design of MEMS systems, energy harvesters, and metastructures.

Appendix: Boundary Conditions and Mode Shape Constants

The boundary condtions and constant values for the linear mode shapes of different boundary conditions are shown in Tables 8 and 9. The *P* refers to pinned, *G* refers to guided, and *C* refers to clamped where

Table 8 Boundary conditions

Case	P-P	P-G	G-G	P-C	G-P
BCs	$w_1 = w_1'' = 0$ $w_2 = w_2'' = 0$	$w_1 = w_1'' = 0$ $w_2' = w_2''' = 0$	$w_1' = w_1''' = 0$ $w_2' = w_2''' = 0$	$w_1 = w_1'' = 0$ $w_2 = w_2' = 0$	$w_1' = w_1''' = 0$ $w_2 = w_2' = 0$
Linear BCs	$Y_1 = Y_1'' = 0$ $Y_2 = Y_2'' = 0$	$Y_1 = Y_1'' = 0$ $Y_2' = Y_2''' = 0$	$Y_1' = Y_1''' = 0$ $Y_2' = Y_2''' = 0$	$Y_1 = Y_1'' = 0$ $Y_2 = Y_2' = 0$	$Y_1' = Y_1''' = 0$ $Y_2 = Y_2' = 0$
Nonlinear BCs	$\phi_1 = \phi_1'' = 0$ $\phi_2 = \phi_2'' = 0$	$\phi_1 = \phi_1'' = 0$ $\phi_2' = \phi_2''' = 0$	$\phi_1' = \phi_1''' = 0$ $\phi_2' = \phi_2''' = 0$	$\phi_1 = \phi_1'' = 0$ $\phi_2 = \phi_2 = 0$	$\phi_1' = \phi_1''' = 0$ $\phi_2 = \phi_2 = 0$

Table 9 Constant values for the linear mode shapes in terms of *c*

		Pinned-pinned	
c_{11}	1	c_{12}	$\frac{\sin\beta\xi_{s1}}{\sin\beta\xi_{s2}}$
c_{21}	0	c_{22}	0
c_{31}	γ_{pp}	c_{32}	$\frac{\sinh\beta\xi_{s1}}{\sinh\beta\xi_{s2}}\gamma_{pp}$
c_{41}	0	c_{42}	0
		Pinned-guided	
c_{11}	1	c_{12}	0
c_{21}	0	c_{22}	$\frac{\sin\beta\xi_{s1}}{\cos\beta\xi_{s2}}$
c_{31}	γ_{pg}	c_{32}	0
c_{41}	0	c_{42}	$\frac{\sinh\beta\xi_{s1}}{\cosh\beta\xi_{s2}}\gamma_{pg}$
		Guided-guided	
c_{11}	0	c_{12}	0
c_{21}	1	c_{22}	$\frac{\cos\beta\xi_{s1}}{\cos\beta\xi_{s2}}$
c_{31}	0	c_{32}	0
c_{41}	γ_{gg}	c_{42}	$\frac{\cosh\beta\xi_{s1}}{\sinh\beta\xi_{s2}}\gamma_{gg}$
		Pinned-clamped	
c_{11}	1	c_{12}	$\frac{1}{\gamma_{pc}}(\cosh\beta\sin\beta\xi_{s1} + \sinh\beta\xi_{s1}\cos\beta)$
c_{21}	0	c_{22}	$\frac{1}{\gamma_{pc}}(\sin\beta\sinh\beta\xi_{s1} - \sin\beta\xi_{s1}\sinh\beta)$
c_{31}	$\frac{1}{\gamma_{pc}}(\cos\beta\sinh\beta\xi_{s2} + \sin\beta\xi_{s1} - \cosh\beta\xi_{s2}\sin\beta)$	c_{32}	$-c_{12}$
c_{41}	0	c_{42}	$-c_{22}$
		Guided-clamped	
c_{11}	0	c_{12}	$\frac{1}{\gamma_{gc}}(\sin\beta\cosh\beta\xi_{s1} + \cos\beta\xi_{s1}\sinh\beta)$
c_{21}	1	c_{22}	$\frac{1}{\gamma_{gc}}(\cosh\beta\cos\beta\xi_{s1} + \cosh\beta\xi_{s1}\cos\beta)$
c_{31}	0	c_{32}	$-c_{12}$
c_{41}	$\frac{1}{\gamma_{gc}}(\sin\beta\sinh\beta\xi_{s2} - \cos\beta\xi_{s1} + \cosh\beta\xi_{s2}\cos\beta)$	c_{42}	$-c_{22}$

$$\gamma_{pp} = \frac{\cot\ \beta\xi_{s2} + \cos\ \beta\xi_{s1}}{\cosh\ \beta\xi_{s1} - \coth\ \beta\xi_{s2}\sinh\ \beta\xi_{s1}} \tag{A1}$$

$$\gamma_{pg} = \frac{\cos\ \beta\xi_{s1} + \sin\ \beta\xi_{s1}\tan\ \beta\xi_{s2}}{\cosh\ \beta\xi_{s1} - \tanh\ \beta\xi_{s2}\sinh\ \beta\xi_{s1}} \tag{A2}$$

$$\gamma_{gg} = \frac{\sin\ \beta\xi_{s1} + \tan\ \beta\xi_{s2}\cos\ \beta\xi_{s1}}{\sinh\ \beta\xi_{s1} - \tanh\ \beta\xi_{s2}\cosh\ \beta\xi_{s1}} \tag{A3}$$

$$\gamma_{pc} = \sinh\ \beta\xi_{s1} + \sin\ \beta\xi_{s2}\cosh\ \beta - \cos\ \beta\xi_{s2}\sinh\ \beta \tag{A4}$$

$$\gamma_{gc} = \cosh\ \beta\xi_{s1} + \sin\ \beta\xi_{s2}\sinh\ \beta - \cos\ \beta\xi_{s2}\cosh\ \beta \tag{A5}$$

References

[1] Lu, Z., Wang, Z., Zhou, Y., and Lu, X., 2018, "Nonlinear Dissipative Devices in Structural Vibration Control: A Review," J. Sound Vib., **423**, pp. 18–49.

[2] Vakakis, A. F., Gendelman, O. V., Bergman, L. A., McFarland, D. M., Kerschen, G., and Lee, Y. S., 2008, *Nonlinear Targeted Energy Transfer in Mechanical and Structural Systems*, Vol. 156, Springer Science & Business Media, New York.

[3] Bukhari, M. A., and Barry, O. R., 2018, "Nonlinear Vibrations Analysis of Overhead Power Lines: A Beam With Mass–Spring–Damper–Mass Systems," ASME J. Vib. Acoust., **140**(3), p. 031004.

[4] Vaurigaud, B., Manevitch, L. I., and Lamarque, C.-H., 2011, "Passive Control of Aeroelastic Instability in a Long Span Bridge Model Prone to Coupled Flutter Using Targeted Energy Transfer," J. Sound Vib., **330**(11), pp. 2580–2595.

[5] Lee, Y., Vakakis, A., Bergman, L., McFarland, D. M., and Kerschen, G., 2007, "Suppression Aeroelastic Instability Using Broadband Passive Targeted Energy Transfers—Part 1: Theory," AIAA J., **45**(3), pp. 693–711.

[6] Hubbard, S. A., Fontenot, R. L., McFarland, D. M., Cizmas, P. G., Bergman, L. A., Strganac, T. W., and Vakakis, A. F., 2014, "Transonic Aeroelastic Instability Suppression for a Swept Wing by Targeted Energy Transfer," J. Aircr., **51**(5), pp. 1467–1482.

[7] Ebrahimzade, N., Dardel, M., and Shafaghat, R., 2016, "Performance Comparison of Linear and Nonlinear Vibration Absorbers in Aeroelastic Characteristics of a Wing Model," Nonlinear Dyn., **86**(2), pp. 1075–1094.

[8] Woinowsky-krieger, S., 1950, "The Effect of an Axial Force on the Vibration of Hinged Bars," ASME J. Appl. Mech., **17**(1), pp. 35–36.

[9] Burgreen, D., 1950, "Free Vibrations of a Pin-Ended Column With Constant Distance Between Pin Ends," Polytechnic Inst of Brooklyn, Brooklyn, NY, Report No. AD0494776.

[10] Bennett, J. A., 1973, "Ultraharmonic Motion of a Viscously Damped Nonlinear Beam," AIAA J., **11**(5), pp. 710–715.

[11] Nayfeh, A. H., and Mook, D., 1979, *Nonlinear Oscillations*, John Willey and Sons, New York.

[12] Nayfeh, A. H., 2011, *Introduction to Perturbation Techniques*, Wiley, New York.

[13] Dowell, E., 1980, "Component Mode Analysis of Nonlinear and Nonconservative Systems," ASME J. Appl. Mech., **47**(1), pp. 172–176.

[14] Pakdemirli, M., and Nayfeh, A., 1994, "Nonlinear Vibrations of a Beam-Spring-Mass System," ASME J. Vib. Acoust., **116**(4), pp. 433–439.

[15] Barry, O., Oguamanam, D., and Zu, J., 2014, "Nonlinear Vibration of an Axially Loaded Beam Carrying Multiple Mass–Spring–Damper Systems," Nonlinear Dyn., **77**(4), pp. 1597–1608.

[16] Bukhari, M. A., and Barry, O. R., 2017, "Nonlinear Vibrations of a Beam-Spring-Large Mass System," ASME Paper No. IMECE2017-70444.

[17] Low, K., 1997, "Comments on"Non-Linear Vibrations of a Beam-Mass System Under Different Boundary Conditions," J. Sound Vib., **207**(2), pp. 284–287.

[18] Mestrom, R., Fey, R., Phan, K., and Nijmeijer, H., 2010, "Simulations and Experiments of Hardening and Softening Resonances in a Clamped–Clamped Beam Mems Resonator," Sens. Actuators A: Phys., **162**(2), pp. 225–234.

[19] Özkaya, E., and Pakdemirli, M., 1999, "Non-Linear Vibrations of a Beam–Mass System With Both Ends Clamped," J. Sound Vib., **221**(3), pp. 491–503.

[20] Özkaya, E., Pakdemirli, M., and Öz, H., 1997, "Non-Linear Vibrations of a Beam-Mass System Under Different Boundary Conditions," J. Sound Vib., **199**(4), pp. 679–696.

[21] Özkaya, E., 2002, "Non-Linear Transverse Vibrations of a Simply Supported Beam Carrying Concentrated Masses," J. Sound Vib., **257**(3), pp. 413–424.

[22] Roncen, T., Sinou, J.-J., and Lambelin, J., 2018, "Non-Linear Vibrations of a Beam With Non-Ideal Boundary Conditions and Uncertainties–Modeling, Numerical Simulations and Experiments," Mech. Syst. Signal Process., **110**, pp. 165–179.

[23] Zhang, W., Ma, H., Zeng, J., Wu, S., and Wen, B., 2017, "Vibration Responses Analysis of an Elastic-Support Cantilever Beam With Crack and Offset Boundary," Mech. Syst. Signal Process., **95**, pp. 205–218.

[24] Abbasnejad, B., and Rezazadeh, G., 2012, "Mechanical Behavior of a Fgm Micro-Beam Subjected to a Nonlinear Electrostatic Pressure," Int. J. Mech. Mater. Des., **8**(4), pp. 381–392.

[25] Younis, M. I., Alsaleem, F., and Jordy, D., 2007, "The Response of Clamped–Clamped Microbeams Under Mechanical Shock," Int. J. Non-Linear Mech., **42**(4), pp. 643–657.

[26] Mojahedi, M., Zand, M. M., Ahmadian, M., and Babaei, M., 2011, "Analytic Solutions to the Oscillatory Behavior and Primary Resonance of Electrostatically Actuated Microbridges," Int. J. Struct. Stability Dyn., **11**(06), pp. 1119–1137.

[27] Xu, T., Ruzziconi, L., and Younis, M. I., 2017, "Global Investigation of the Nonlinear Dynamics of Carbon Nanotubes," Acta Mech., **228**(3), pp. 1029–1043.

[28] Yuan, P.-P., Ren, W.-X., and Zhang, J., 2019, "Dynamic Tests and Model Updating of Nonlinear Beam Structures With Bolted Joints," Mech. Syst. Signal Process., **126**, pp. 193–210.

[29] Samani, F. S., and Pellicano, F., 2009, "Vibration Reduction on Beams Subjected to Moving Loads Using Linear and Nonlinear Dynamic Absorbers," J. Sound Vib., **325**(4–5), pp. 742–754.

[30] Samani, F. S., and Pellicano, F., 2012, "Vibration Reduction of Beams Under successive traveling Loads by Means of Linear and Nonlinear Dynamic Absorbers," J. Sound Vib., **331**(10), pp. 2272–2290.

[31] Samani, F. S., Pellicano, F., and Masoumi, A., 2013, "Performances of Dynamic Vibration Absorbers for Beams Subjected to Moving Loads," Nonlinear Dyn., **73**(1–2), pp. 1065–1079.

[32] Haxton, R. S., and Barr, A. D. S., 1972, "The Autoparametric Vibration Absorber," ASME J. Eng. Ind., **94**(1), pp. 119–125.

[33] Silva-Navarro, G., and Abundis-Fong, H. F., 2015, "Passive/Active Autoparametric Cantilever Beam Absorber With Piezoelectric Actuator for a Two-Story Building-Like Structure," ASME J. Vib. Acoust., **137**(1), p. 011017.

[34] Tan, T., Yan, Z., Zou, Y., and Zhang, W., 2019, "Optimal Dual-Functional Design for a Piezoelectric Autoparametric Vibration Absorber," Mech. Syst. Signal Process., **123**, pp. 513–532.

[35] Avramov, K., and Gendelman, O., 2010, "On Interaction of Vibrating Beam With Essentially Nonlinear Absorber," Meccanica, **45**(3), pp. 355–365.

[36] Pohit, G., Mallik, A., and Venkatesan, C., 1999, "Free Out-of-Plane Vibrations of a Rotating Beam With Non-Linear Elastomeric Constraints," J. Sound Vib., **220**(1), pp. 1–25.

[37] Das, S., Ray, P., and Pohit, G., 2005, "Large Amplitude Free Vibration Analysis of a Rotating Beam With Non-Linear Spring and Mass System," Modal Anal., **11**(12), pp. 1511–1533.

[38] Das, S., Ray, P., and Pohit, G., 2007, "Free Vibration Analysis of a Rotating Beam With Nonlinear Spring and Mass System," J. Sound Vib., **301**(1–2), pp. 165–188.

[39] Barry, O., Zu, J., and Oguamanam, D., 2015, "Nonlinear Dynamics of Stockbridge Dampers," ASME J. Dyn. Syst., Meas., Control, **137**(6), p. 061017.

[40] Nayfeh, A. H., 1995, "On Direct Methods for Constructing Nonlinear Normal Modes of Continuous Systems," Modal Anal., **1**(4), pp. 389–430.

[41] Lin, H.-Y., and Tsai, Y.-C., 2007, "Free Vibration Analysis of a Uniform Multi-Span Beam Carrying Multiple Spring–Mass Systems," J. Sound Vib., **302**(3), pp. 442–456.

[42] Malatkar, P., and Nayfeh, A. H., 2006, "Steady-State Dynamics of a Linear Structure Weakly Coupled to an Essentially Nonlinear Oscillator," Nonlinear Dyn., **47**(1–3), pp. 167–179.

[43] Ji, J., 2012, "Application of a Weakly Nonlinear Absorber to Suppress the Resonant Vibrations of a Forced Nonlinear Oscillator," ASME J. Vib. Acoust., **134**(4), p. 044502.

[44] Sedighi, H. M., Shirazi, K. H., and Attarzadeh, M. A., 2013, "A Study on the Quintic Nonlinear Beam Vibrations Using Asymptotic Approximate Approaches," Acta Astronaut., **91**, pp. 245–250.

[45] Wu, J.-S., and Chou, H.-M., 1999, "A New Approach for Determining the Natural Frequencies and Mode Shapes of a Uniform Beam Carrying Any Number of Sprung Masses," J. Sound Vib., **220**(3), pp. 451–468.